scientific reports

Check for updates

OPEN

Origin of metamagnetism in skyrmion host Cu_2OSeO_3

Harish Chandr Chauhan, Birendra Kumar & Subhasis Ghosh✉

Skyrmion host chiral Cu_2OSeO_3 has attracted researchers due to several intriguing properties. Observation of metamagnetism in low-temperature and low-field makes the magnetic properties of Cu_2OSeO_3 more complex. Here, we present an investigation on metamagnetism in Cu_2OSeO_3 by analyzing its structural and magnetic properties. Study of magnetic properties reveal spin-flip of one of the Cu^{2+} ions, embedded in square pyramidal CuO_5 polyhedra, due to the development of strain in low-temperature and low-field regime. The spin-flip is found to be the main reason for field-induced first-order metamagnetic transition. Magnetic phase diagram of Cu_2OSeO_3 has been constructed with the help of magnetization analyses. It is argued that the metamagnetic hysteretic field region may be low-temperature skyrmion phase with additional spiral and tilted-conical phases. A tricritical point has been observed in the phase diagram at which first-order metamagnetic hysteretic field range ceases to exist.

Skyrmion, a vortex like spin-texture, has been observed in various magnetic systems having different crystal symmetries[1–14]. Skyrmion host magnetic systems are good candidate for information carriers and magnetic memory devices[15–17]. Generally, skyrmions are observed in centrosymmetric and noncentrosymmetric magnetic materials in a small window of applied field and temperature[1,2,4,11]. In centrosymmetric systems, magnetic bubbles, which are topologically equivalent to skyrmion phase, emerge due to competition between symmetric exchange interaction (SEI) and dipole-dipole interaction[12,13,18,19] under external magnetic field. So, it is important to study the nature of SEI, *i.e*, whether it is Heisenberg type, Ising type or some other type. In noncentrosymmetric magnetic systems[1–8], skyrmions emerge due to competition between SEI and antisymetric-Dzyloshinskii-Moria interaction (DMI)[20,21] under external magnetic field. Multiple magnetic phases, such as helical, conical, field polarized (FP) and fluctuation disordered (FD), also evolve with temperature under external magnetic field[1–8]. Skyrmion phase emerges in a small pocket of applied field and temperature. So, a general Hamiltonian, which is responsible for the formation of various magnetic phases, can be written as

$$\begin{aligned}\mathscr{H} &= \mathscr{H}_{SEI} + \mathscr{H}_{DMI} + \mathscr{H}_{d} + \mathscr{H}_{Ani} + \mathscr{H}_{Zeeman} \\ &= \sum_{ij} J_{ij}\mathbf{S}_i.\mathbf{S}_J + \sum_{ij} \mathbf{D}_{ij}.(\mathbf{S}_i \times \mathbf{S}_j) + K_d \sum_{ij} \left(3\frac{(\mathbf{S}_i.\mathbf{r}_{ij})(\mathbf{S}_j.\mathbf{r}_{ij})}{r_{ij}^5} - \frac{\mathbf{S}_i.\mathbf{S}_j}{r_{ij}^3}\right) + \mathscr{H}_{Ani} - \mu_0\mathbf{H}.\mathbf{M}. \end{aligned} \quad (1)$$

where $\mathscr{H}_{SEI}$, $\mathscr{H}_{DMI}$, $\mathscr{H}_{d}$, $\mathscr{H}_{Ani}$ and $\mathscr{H}_{Zeeman}$ are the Hamiltonian for SEI, DMI, dipole-dipole interaction[13,22,23], anisotropic interaction and Zeeman interaction, respectively. J_{ij} is the coefficient of exchange interaction, $\mathbf{D}_{ij}$ is Dzyaloshinskii-Moriya vector and K_d is the coefficient of dipole-dipole interaction. The dipolar energy is effective in low dimension, such as two-dimension (2D)[22], thin-films[23] and layered systems[13]. In bulk systems, dipolar energy is negligibly small[24]. That is why, in noncentrosymmetric chiral cubic systems, dipolar energy is generally neglected leading to $K_d = 0$[25–27]. In centrosymmetric magnetic systems $\mathbf{D}_{ij} = 0$[21]. $\mathscr{H}_{Ani}$ is highly dependent on the chosen system which is why expression for $\mathscr{H}_{Ani}$ is not given[28–34]. In Cu_2OSeO_3, magnetocrystalline anisotropy, with easy axis along [111], plays key role in various physical phenomena[35–37]. The exchange coefficient J_{ij} also varies with chosen materials. For example, the physics of MnSi and FeGe are governed by single value of J while the physics of Cu_2OSeO_3 is governed by using at least four values of J depending on the chosen Cu^{2+} ions[25–27]. The magnetic phase diagram of several skyrmion host magnetic materials have been reported with the help of various techniques such as Lorentz transmission electron microscopy (LTEM)[4], small-angle neutron scattering (SANS)[4], specific heat[38], magnetic susceptibility[38] and magnetic isotherm[39,40]. A detailed investigation on different phases and phase transition between them has made it possible to explore the existence of various critical points such as Lifshitz point[40], tricritical point[38,40], and triple point[41].

Cu_2OSeO_3 is the only known magnetic material in which the skyrmion phase has been observed in two different pockets of applied field and temperature[35,42–45]. High-temperature skyrmion (HTS) phase has been

School of Physical Sciences, Jawaharlal Nehru University, New Delhi 110067, India. ✉email: subhasis.ghosh.jnu@gmail.com

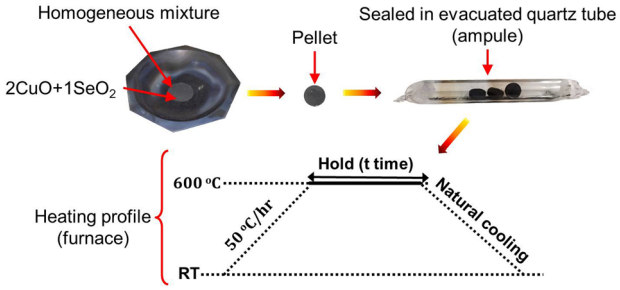

Figure 1. Schematic representation of the synthesis of Cu_2OSeO_3. First, homogeneous mixture of CuO and SeO_2 was taken in the molar ratio of 2:1, respectively. Then, pellets were made using hydraulic pressure and sealed in an evacuated quartz tube. The heating profile of the reaction was performed as the given schematic cycle. Intermediate grindings were performed to achieve single phase of the sample. RT: room temperature.

observed in the vicinity of $T_C(\simeq 59\,K)$, and the low-temperature skyrmion (LTS) phase has been observed in low-temperature regime ($T << T_C$). As discussed above, the competition among SEI, DMI, magnetocrystalline anisotropy, thermal energy and Zeeman energy give rise to skyrmion and other phases. So, it is natural to ask–How skyrmions emerge at two different pockets of applied field and temperature? Interestingly, the properties of HTS and LTS are different[35,42–45]. The SANS results show–six-fold intensity pattern for HTS while ring plus six-fold intensity pattern for LTS phase[35,42,44]. The LTS phase has been observed only along [100] direction[44] hinting the lowering of cubic symmetry due to some structural deformation, such as the emergence of magnetoelastic anisotropy which leads to completely different scenario of competing energies. So, the Hamiltonian (Eq. 1) should be different for HTS and LTS phases. Moreover, similar SANS result (ring plus six-fold intensity pattern) has been observed for FD phase in MnSi[46,47]. It has been investigated that the FD phase is thermally induced chiral fluctuations caused by first-order Brazovskii transition[48]. However, the explained physics for LTS is completely different from the physics for FD phase in spite of having almost similar SANS results. It is concluded that rings intensity pattern may arise from thermodynamically stable skyrmionic correlation, which coexist with spiral and tilted-conical phases[42]. Also, the sudden jump in the magnetization isotherm with hysteresis has been observed in Cu_2OSeO_3 at low-temperature ($T << T_C$), and is known as metamagnetic transition[49]. More importantly, the LTS phase emerges in the metamagnetic hysteretic field range (has been discussed in detail later). Bannenberg *et al.*[42] have explained the physics of different spin-textures with theoretical investigation by incorporating strength of cubic anisotropy. Here, the important question is– How does metamagnetic behavior appear in Cu_2OSeO_3? Thus, the observation of skyrmion in two different pockets of applied field and temperature, and several other novel magnetic phases, more importantly, the manipulation of skyrmions with an electric field[50], necessitates the further investigation of metamagnetism in Cu_2OSeO_3[49]. Generally, the materials showing metamagnetism undergo first-order phase transition from the state of low magnetic moment to the state of the high magnetic moment in the presence of magnetic field[51–53]. Metamagnetism has been observed in various magnetic systems having different structural properties such as linear chain systems, two sublattice systems, four sublattice systems, garnets and mixed crystals[54]. Metamagnetic transitions have been observed in: (i) highly anisotropic systems due to local spin reversal, and (ii) isotropic or weak anisotropic systems due to the rotation of local spin directions[54]. Cu_2OSeO_3 has two types of CuO_5 polyhedra – square pyramidal and trigonal bipyramidal in the ratio of 3:1 – which leads to the formation of two sublattices[4]. As discussed above, formation of two sublattices causes the emergence of the magnetocrystalline anisotropy in the system with easy axis along [111][35–37]. Thus, below T_C, the phase transition and the critical phenomena will be facilitated by SEI, DMI and anisotropies. Also, there should exist a tricritical point at which metamagnetic behavior disappears, leading to a continuous variation of magnetization. The physics of the metamagnetic properties of Cu_2OSeO_3 with associated tricritical point has not been explored yet.

Here, we present investigation on the origin of metamagnetism by incorporating structural and magnetic analyses of skyrmion host Cu_2OSeO_3. It is found that spin-flip of one of Cu^{2+} ions (embedded with aquare pyramidal polyhedra) is the main reason for metamagnetism. The possible spin textures of metamagnetic hysteretic field range has been discussed comprehensively. A complete phase diagram of Cu_2OSeO_3 has been presented. A tricritical point, where first-order metamagnetic hysteretic field range ceases to exist and second-order helical to conical phase transition emerges, has been found.

Experimental details

Cu_2OSeO_3 was grown using solid–state reaction method[40]. High purity CuO (Sigma Aldrich 99.999 %) and SeO_2 (Sigma Aldrich 99.999 %) were taken in the molar ratio of 2:1, respectively. The mixture of CuO and SeO_2 were grinded together for at least 8 hrs to obtain the homogeneous mixture. After making pellets of the homogeneous mixture, the sample was sealed in an evacuated quartz tube, which was then placed into a muffle furnace and annealed at 600 °C with heating rate of 50 °C/hr. The sample was held at 600 °C for 5 weeks. The intermediate grinding was performed for phase purity of the sample. Figure 1 represents experimental procedure used for the synthesis of Cu_2OSeO_3 sample. The X-ray diffraction (XRD) data of Cu_2OSeO_3 were collected using Rigaku Miniflex 600 X-Ray Diffractometer with Cu–K_α radiation. Phase purity of the sample was confirmed using Rietveld refinement of the XRD data[40]. High precision magnetic measurements were performed using physical

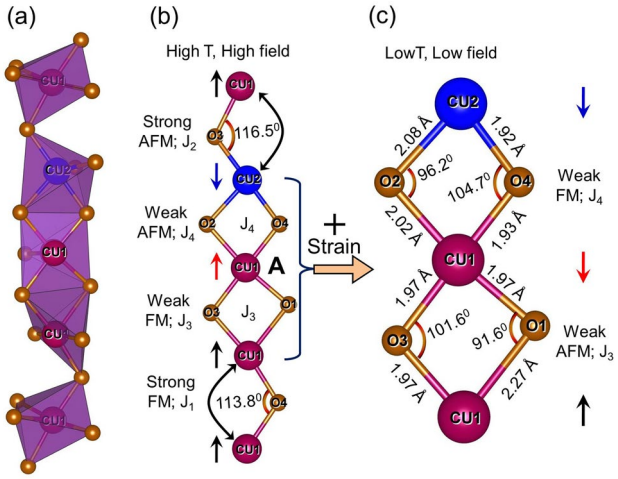

Figure 2. (**a**) Single lattice chain of CuO_5 polyhedra. Square pyramidal (around Cu1) and trigonal bipyramidal (around Cu2) CuO_5 polyhedra are present in the crystal structure in the ratio of 3:1. The lattice constant of the cubic crystal structure of Cu_2OSeO_3 is $a = 8.922$ Å. (**b**) Single lattice chain of Cu–O–Cu bonding. $J_1 = -3.693$ meV and $J_3 = -1.132$ meV are ferromagnetic superexchange couplings. $J_2 = 6.534$ meV and $J_4 = 0.900$ meV are antiferromagnetic superexchange couplings. These J values have been assigned from Ref.[25]. The directions of spins are shown schematically. (**c**) Edge sharing polyhedra showing weak AFM and weak FM. This is the most probable structure which can crossover from weak FM to weak AFM and vice versa with the development of magnetoelastic anisotropy which causes development of strain in the material.

properties measurement system. Field cooled (FC) and zero field cooled (ZFC) magnetization data were collected at 10, 20, 40 and 100 mT in warming mode. Four-quadrant field-dependent magnetization (M-H) isotherms were collected up to 250 mT at 2, 10, 20, 30, 40, 50, 57, 60, and 70 K. The step increment of the field was 1 mT. The magnetization data were recorded via following process: (i) first forward scan from 0 to 250 mT, (ii) first reverse scan from 250 to −250 mT, (iii) second forward scan from −250 to 250 mT, and (iv) second reverse scan from 250 to 0 mT. The analyses of Arrott-plots, susceptibility and phase diagram were carried out using the first-quadrant M-H isotherms of the second forward field scan.

Results and discussion

Structural analysis. The cubic crystal structure of Cu_2OSeO_3 with the lattice constant $a = 8.922$ Åwas estimated from the room temperature XRD analysis using Rietveld refinement[40]. Cu_2OSeO_3 lacks inversion symmetry and has 3-fold rotational symmetry along [111] direction. Here, square pyramidal (around Cu1) and trigonal bipyramidal (around Cu2) polyhedra are in the ratio of 3:1 as shown in Fig. 2a. The unequal ratio of Cu1 and Cu2 result in the formation of local ferrimagnetic ordering[4,41]. Figure 2b shows a simple lattice chain of Cu–O–Cu atoms estimated from the crystal structure. These lattice chains exhibit in the form of trigonal pyramid in which each lattice chain resides at the edges of the pyramid. In a single unit cell of Cu_2OSeO_3 ($a = 8.922$ Å), each lattice chain consists of three Cu1 and one Cu2 atom. J_1 and J_2 are the superexchange couplings (Fig. 2b) between Cu atoms connected with corner-sharing CuO_5 polyhedra as shown in Fig. 2a. J_3 and J_4 are the superexchange couplings (Fig. 2b) between Cu atoms connected with edge-sharing CuO_5 polyhedra as shown in Fig. 2a. Zhang et al.[55] suggested that the edge-sharing Cu–O–Cu atoms have weaker exchange interaction than the corner-sharing. This means J_1 and J_2 are stronger than J_3 and J_4. They have also indicated that the interaction between two identical atoms having different environment favors antiferromagnetic (AFM) exchange coupling while the interaction between two identical atoms having similar environment favor ferromagnetic (FM) exchange coupling as shown in Fig. 2b. Yang et al.[25] have investigated the strengths of the superexchange couplings present in Cu_2OSeO_3. Following the above arguments and using the results of Yang et al.[25], we can assign values to different superexchange couplings as $J_1 = -3.693$ meV, $J_2 = 6.534$ meV, $J_3 = -1.132$ meV, and $J_4 = 0.900$ meV. Other groups have also estimated the values of the exchange couplings[26,27]. The estimated values from other groups[26,27] are slightly different but the nature of the exchange couplings is same. It has been reported that the edge-sharing superexchange coupling may alter its coupling behavior (from weak FM to weak AFM and vice versa)[56]. Further discussions are carried out in the coming sections about–How spin-flip may occur in Cu_2OSeO_3?

Magnetic analysis. *Temperature-dependent magnetization.* Figure 3a shows the temperature-dependent magnetization (M-T) of Cu_2OSeO_3 taken at 10, 20, 40, and 100 mT. The minimum of the first derivative $\left(\frac{dM}{dT}\right)$ of the ZFC M-T isofields (Fig. 3b) yield $T_C \approx 59.10$, 58.95, 58.88, and 59.50 K at 10, 20, 40, and 100 mT, respectively. The $\frac{dM}{dT}$ at 10 and 20 mT show peak at 57.4 and 57.78 K (Fig. 3b), respectively. These transition points are consistent with the phase boundary of FD regime[40], which is known as the precursor phase for the formation of

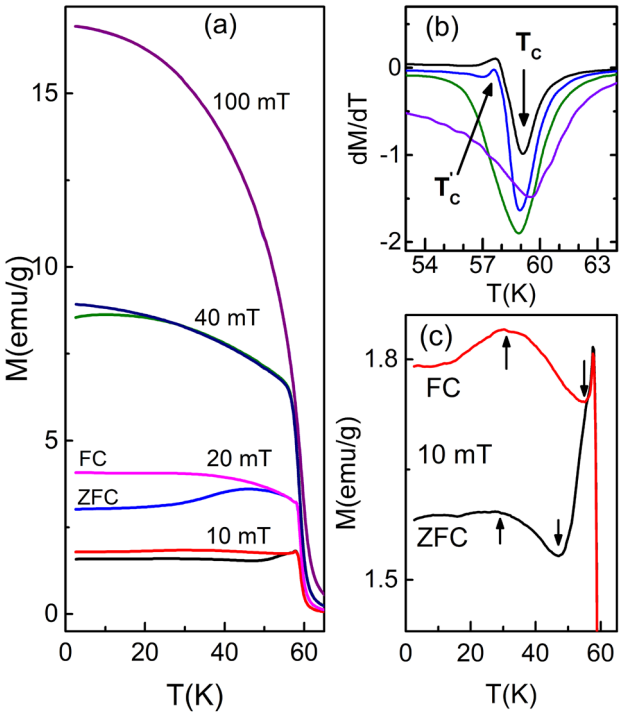

Figure 3. (**a**) FC and ZFC plots of the temperature-dependent magnetization (M-T) data taken at various applied magnetic fields as mentioned. (**b**) The first derivative of the ZFC curves. The minimum of the first derivative of the M-T plots give transition temperatures. An anomaly is observed in the derivatives of 10 and 20 mT. These transition points are consistent with the FD phase boundary. A complete field polarized ferrimagnetic ordering is observed at 100 mT. (**c**) Expanded view of the M-T curves taken at 10 mT.

helimagnetic spin textures in skyrmion host magnetic materials[38,40,57]. The bifurcation in the FC and ZFC M-T isofields are observed till 40 mT (Fig. 3a). Such a typical bifurcation occurs when the applied magnetic field is not enough to break and align the randomly bound magnetic moments in the direction of field. This effect is generally observed due to the presence of magnetocrystalline anisotropy in the system[35–37,58]. The strength of magnetocrystalline anisotropy decreases continuously with increasing temperature. In other words, the bifurcation width (ΔM), which is the difference between the magnetic moment of FC and ZFC M-T isofields, should decrease with increasing temperature. In helimagnetic materials, domain wall trapping causes bifurcation in the M-T isofields and formation of hysteresis around origin in the M-H isotherms[59–61]. As observed in Fig. 3a, ΔM is less at 10 mT, and maximum at 20 mT. Also, ΔM increases with temperature at low applied field (Fig. 3c). Thus, the variation of ΔM is unusual in the context of magnetocrystalline anisotropy. This leads to the conclusion that there should exists some other anisotropy to compete with magnetocrystalline anisotropy. It seems that exchange anisotropy, which may cause spin-reversal, is locally effective at low-temperature and low-field in Cu_2OSeO_3.

The variation of FC and ZFC M-T taken at 10 mT is shown in Fig. 3c. In the vicinity of T_C, the cusp like behavior is observed due to the competitive effect of antisymmetric DMI and SEI. Similar kind of cusp has been observed in other chiral cubic B20 materials in which the physics is governed by single FM exchange coupling[62–64]. The M-T taken at 10 mT (Fig. 3c) shows unusual variation in comparison with the M-T of other skyrmionic hosts B20 materials[62–64]. In FC warming mode, the magnetic moment: (i) increases from 2 to 31 K, (ii) decreases from 31 to 55 K, (iii) further increases from 55 K to 57.7 K, and (iv) finally decreases to zero. This means the multiple superexchange couplings are causing such unusual variation[25]. The ZFC M-T taken at 10 mT (Fig. 3c) also shows similar unusual variation. In the absence of external magnetic field, magnetocrystalline anisotropy plays an important role by driving the magnetic moment along the easy axes. The magnetization at 10 mT shows following temperature-dependence in ZFC warming mode. The magnetic moment: (i) increases from 2 to 29 K, (ii) decreases from 29 to 47 K, (iii) further increases from 47 to 57.7 K, and (iv) finally decreases to zero. Below 31 K, the FC M-T looks alike the M-T for weak AFM material[65,66]. But, the variation of M-T does not reflect pure AFM variation due to presence of DMI, anisotropy energies and Zeeman energy. The above arguments lead to the conclusion that the crossover occurs from weak FM (in high temperature regime) to weak AFM (in low temperature regime) resulting small reduction in the magnetic moment. The crossover will occur only if one of the Cu spins get flipped which will cause change in effective anisotropies. The flipping of those spins, which are connected with weaker exchange couplings, is more favorable. So, the spins connected by J_3 and J_4 are most probable to get flipped resulting in the lowering of the magnetic moment. Mondal et al.[56] have suggested that the change in the Cu–O–Cu bond angle may cause a crossover of the exchange coupling from FM to AFM and vice versa. The same crossover is possible in Cu_2OSeO_3 if strain develops at low temperature (see Fig. 2c). Bos et al.[49] and Evans et al.[67] have shown how strain indeed develops at low temperature in Cu_2OSeO_3. Thus,

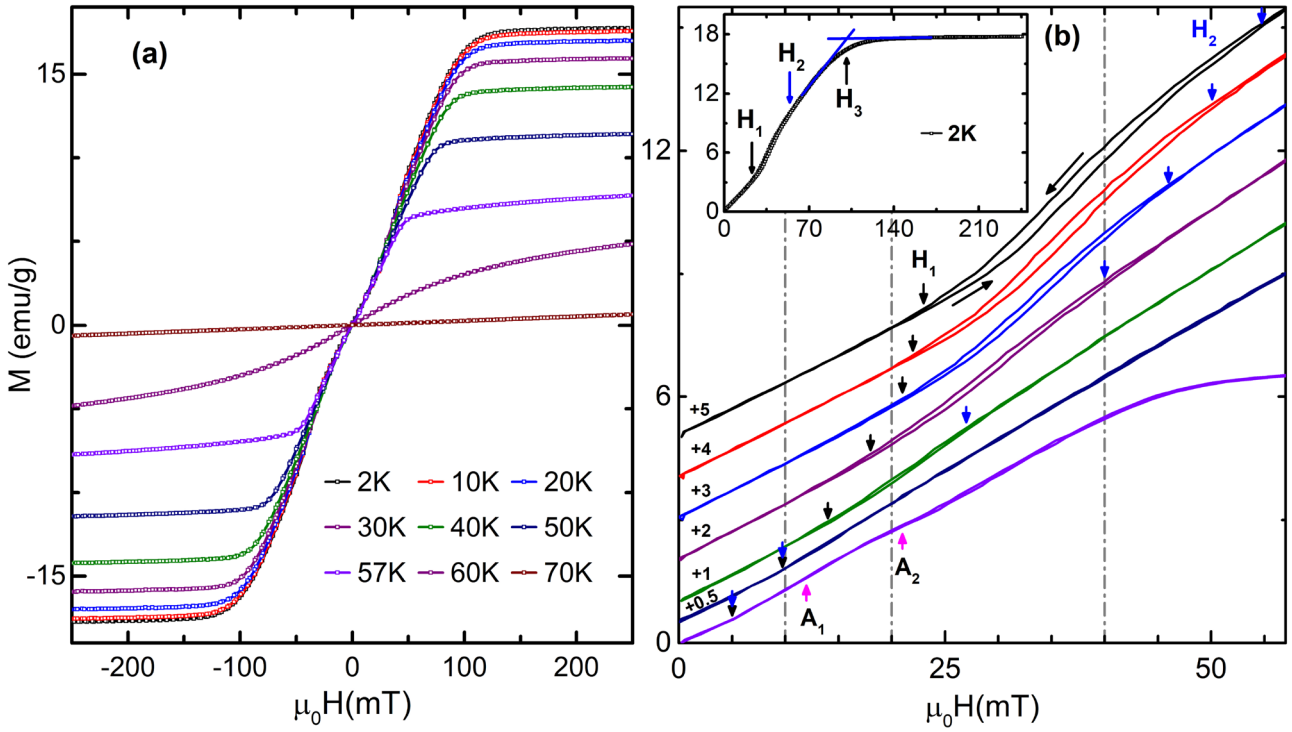

Figure 4. (**a**) M-H isotherms measured in the step mode up to 250 mT with increment step of 1 mT taken at various temperatures as mentioned. An unusual anomaly of magnetization variation is visible. (**b**) Expanded view of (**a**) to see the clear variation of M-H isotherms. The M-H isotherms have been shifted vertically as mentioned. The first forward scan (0–250 mT) isotherms is not shown due to substantial overlap with the M-H isotherms taken during second forward scan (−250 to 250 mT). There is no magnetic hysteresis around the origin. The metamagnetic hysteresis is observable from 2 to 40 K in the intermediate applied field range H_1 to H_2. The M-H data taken at 57 K shows step-like variation, which is related to skyrmion formation in Cu_2OSeO_3. A_1 and A_2 represent the skyrmion phase boundary. The inset of (**b**) represents the critical field H_3, above which field-induced ferrimagnetic phase has been observed.

the strain developed will actually cause change in effective anisotropies. The observed cusp has disappeared in the M-T taken at high fields (see Fig. 3a) due to ineffectiveness of DMI[41]. The M-T taken at 20 mT also shows similar variation as discussed for the M-T taken at 10 mT. After a critical field (≈ 40 mT), usual variation in the M-T isofields, which are the confirmation of the FP ferrimagnetic ordering, have been observed. The M-H isotherms have been further analyzed to find out the critical-field and critical-temperature responsible for spin-flip.

Field-dependent magnetization. The saturation magnetization of Cu_2OSeO_3 is ≈ 0.53 μ_B/Cu^{2+} ion[49,68], which is approximately half of the magnetic moment of S = 1/2 spin state (1 μ_B) for each Cu^{2+} ion. This confirms ferrimagnetic spin arrangement [3(up):1(down)] in Cu_2OSeO_3[49] in the FP region. Figure 4 shows the M-H isotherms taken up to 250 mT at various temperatures. The linear variation of magnetic moment is observed at small applied field up to H_1 (Fig. 4b). This is same as the variation of the magnetic moment observed for helical phase[8]. The magnetic moment increases abruptly from H_1 to H_2 (Fig. 4b) forming hysteresis in between. This hysteretic field range decreases with increasing temperature and disappears above 40 K. The transition from the low magnetic moment (below H_1) to high magnetic moment (above H_2) with hysteresis between H_1 and H_2 is the characteristic feature of first-order metamagnetic transition[51–54,69,70]. The sudden jump in the magnetic moment is possible only if some Cu spins are flipped in the direction of the applied field. Based on the strength of superexchange couplings, those Cu spins, which are connected with J_3 and J_4, are more likely to be flipped. This is possible only if strain develops in the low-temperature regime causing change in the effective anisotropies. As discussed before, the saturation magnetic moment is ≈0.53 μ_B/Cu^{2+} due to 3(up):1(down) spin configuration above H_2. This implies that spins are antiferromagnetically coupled due to spin-flip below H_1 and 50 K. The schematic representation of spins is shown in Fig. 2c. The above points lead to the conclusion that Hamiltonian should be different below H_1 and 50 K. All these analyses indicate that spin at position **A** (Fig. 2b) is most likely to be flipped. All the above discussions are consistent with the M-T isofields as shown in Fig. 3. The phase between H_2 and H_3 is the conical phase[8]. The magnetic properties of first-order phase transition[71] indicate that the metamagnetic hysteretic field region may be a mixed phase consisting of both helical and conical spin textures or, some other new phase. In analogy to Ref.[71], a small fraction of conical spin textures will start appearing after H_1, and will increase with increasing field till H_2. Below H_2, small fraction of the helical phase will remain while conical phase fraction will be dominating. Indeed, SANS results show coexistence of LTS phase with spiral and tilted-conical phases[42]. Similar SANS result has been observed for FD phase due to thermally induced chiral fluctuation[46,47]. In the analogy, field-induced continuous spin-flip may cause inhomogeneity in

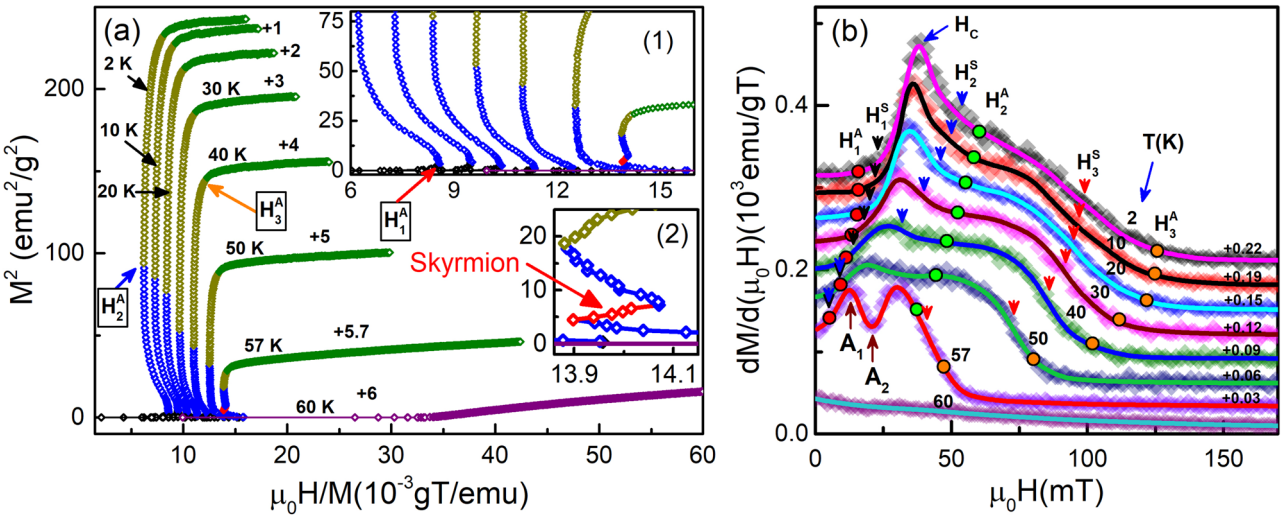

Figure 5. (**a**) Arrott-plots obtained from the first quadrant M-H isotherms recorded during second forward scan from −250 to 250 mT. Various positive and negative slope regions represent multiple phases observed in Cu_2OSeO_3. Inset shows the expanded view of the Arrott-plots. (**b**) Variation of magnetic susceptibility of Cu_2OSeO_3 estimated from the first derivative of the first quadrant M-H isotherms recorded during second forward scan from −250 to 250 mT. Symbols represent experimental data and solid lines are average fit to the experimental data. The phase below H_1^S represents helical phase. Hysteretic phase region is observed between H_1^S and H_2^S. Above H_2^S and up to H_3^S, conical phase formation is estimated. Above H_3^S, field-induced ferrimagnetic phase formation occurs. Flat or almost zero susceptibility value of 60 K curve indicates the paramagnetic phase region.

LTS phase yielding ring intensity pattern along with six-fold intensity pattern in metamagnetic hysteretic field range. After H_2, conical phase will appear till H_3 as shown in the inset of Fig. 4b. Metamagnetic hysteretic phase (and hence metamagnetic transition) is observed below 50 K (see Fig. 4b). Second-order phase transition has been observed[40] from helical to conical phase above 50 K. So the point (50 K, 9 mT) should be the tricritical point at which metamagnetic hysteretic field range ends, and direct helical to conical phase transitions starts. The M-H plot of Cu_2OSeO_3 at 57 K shows the emergence of field-induced HTS phase in the conical phase region[4,8,39,40].

Arrott-plot and susceptibility. Arrott-plot and susceptibility analyses have been further investigated to estimate the phase boundaries connecting different phases present in Cu_2OSeO_3. The Arrott relation[72] is represented as

$$M^2 = A\left(\frac{\mu_0 H}{M}\right) + B, \tag{2}$$

where $A = \frac{1}{b}$ and $B = -\frac{a}{b}$ are constants. Arrott relation[72] is widely used to determine T_C[40] and order of phase transition using Bannerjee's criteria[73]. Figure 5a shows the Arrott-plots obtained using M-H isotherms. As, it can be seen [inset (1) of Fig. 5a] that there exist multiple positive and negative slope regions. Arrott-plots show following properties.

(i) Positive slopes below H_1^A.
(ii) Negative slopes from H_1^A to H_2^A.
(iii) An intermediate positive slope region has been observed between A_1 and A_2 in the negative slope regions (H_1^A to H_2^A) of the Arrott-plot taken at 57 K as shown in the inset(2) of Fig. 5a. The phase between A_1 and A_2 is consistent with observed HTS phase.
(iv) Positive slopes above H_2^A.

The higher field positive slope regions (above H_2^A) can be divided further into two parts– slow varying slope regions (almost vertical lines in Fig. 5a) from H_2^A to H_3^A, and almost constant slope regions above H_3^A. Now, let us first examine the susceptibility plots before going into detailed analysis of different phases appearing in Cu_2OSeO_3. The magnetic susceptibility plot (Fig. 5b), obtained from the first derivative of the M-H isotherms give a clear picture of various transitions. H_1^S, H_2^S and H_3^S are the inflection points on the susceptibility curves below 50 K. The phase boundaries determined from M-H (Fig. 4b) and susceptibility (Fig. 5b) are consistent. Below H_1^S, susceptibility varies linearly, which is consistent with the linear variation of M-H isotherms below H_1 as shown in Fig. 4. On comparison with SANS[4] and LTEM results, the following observation can be made.

(i) Helical phase[1–8] is below H_1^S.

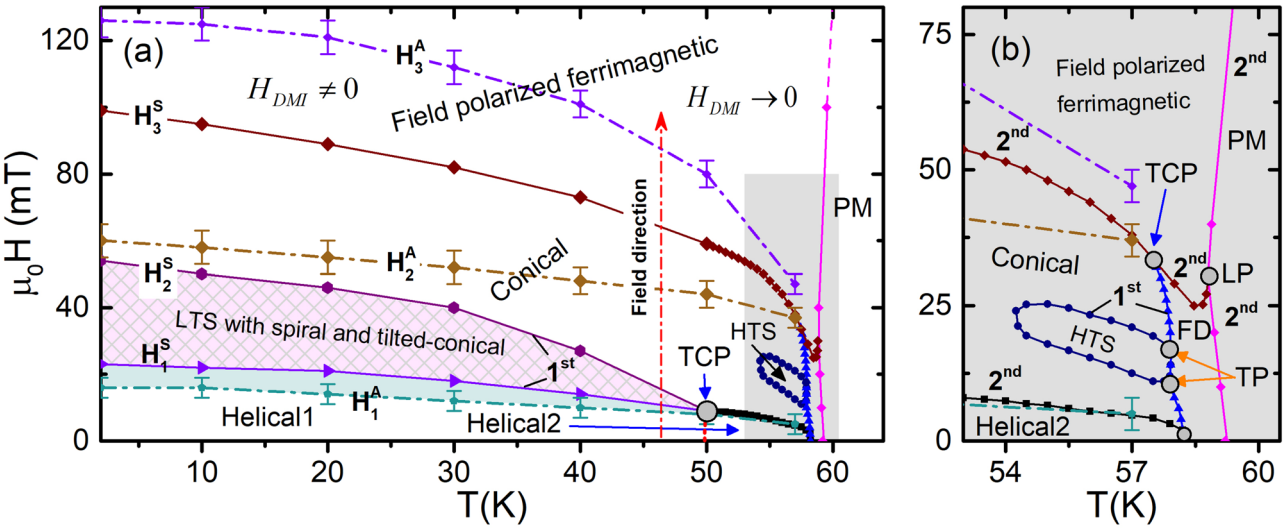

Figure 6. (**a**) Magnetic phase diagram of Cu_2OSeO_3 constructed with the help of FC-ZFC M-T isofields, first quadrant M-H isotherms recorded during second forward scan from −250 to 250 mT, Arrott-plots and susceptibility analyses. H_1^A, H_2^A and H_3^A are the phase boundaries constructed using Arrott-plot (Fig. 5a) analyses. H_1^S, H_2^S and H_3^S are the phase boundaries constructed using magnetic susceptibility (Fig. 5b) analyses. The paramagnetic phase boundary has been constructed using the M-T isofields as depicted in Fig. 3. The HTS phase boundary has been determined using Arrott-plot and susceptibility analyses. Helical phase is below H_1^S. LTS phase with added spiral and tilted conical phase is between H_1^S and H_2^S. Conical phase is from H_2^S to H_3^S. HTS phase has been observed in the vicinity of T_C in conical phase region. FIeld-induced ferrimagnetic phase appears above H_3^S. Here, H_1^A is almost same as H_1^S. H_2^A represents the critical fields around which Arrott-plots change the slope from negative to positive. H_3^A represents the critical fields above which DMI becomes ineffective. (**b**) Expanded view of the shaded (light-gray) region of (**a**). Detailed analysis of the shaded region has been done somewhere else[40]. Helical2, conical, HTS, FP ferrimagnetic, PM and FD phases are observed in the vicinity of T_C. A tricritical point (TCP) is observed at (57.5 K, 33 mT) where first-order FD to conical phase transition transform into second-order conical to field polarized ferrimagnetic phase. Lifshitz point (LP) is observed at (58.8 K, 30 mT) where ordered (FP ferrimagnetic), disordered (PM) and incommensurate (FD) phases meet tangentially. Two triple points (TPs) are observed at [(57.88 K, 17 mT) and (57.90 K, 10.50 mT)] where first-order FD, HTS and conical phases meet. HTS: high-temperature skyrmion, LTS: low-temperature skyrmion, FP: field polarized, FD: fluctuation disordered.

(ii) Conical phase is from H_1^S to H_3^S having intermediate metamagnetic hysteretic field range from H_1^S to H_2^S in low temperature regime. H_C is the critical field where susceptibility is observed to be maximum. The susceptibility pattern from H_1^S to H_2^S is similar to the susceptibility for LTS phase[43], which has been confirmed by SANS results[42,44,45].

(iii) Dip in the susceptibility has been observed from A_1 to A_2 in the conical phase region. The phase between A_1 and A_2 is consistent with the HTS phase[42–45].

(iv) Field induced ferrimagnetic phase appears above H_3^S.

The phase boundaries, constructed using Arrott-plots and susceptibility isotherms, are deviating more in the low temperature regime. H_1^A and H_1^S are almost overlapping in the whole temperature regime. It can be seen that H_2^A is appearing in the conical phase region. With increasing temperature H_2^A and H_3^S get closer to each other. It seems that conical phase is stable till H_3^S and may have different properties below and above H_2^A. After H_3^S, conical phase becomes unstable leading to formation of field induced ferrimagnetic phase having effective DMI till H_3^A. After H_3^A, complete ordered ferrimagnetic phase can be observed with negligibly small DMI[41]. So, the field-region from H_2^A to H_3^A may have mixed spin-textures of conical and field-induced-ferrimagnetic phases. And, spin-textures of conical and field-polarized-ferrimagnetic phases may have equal contribution at H_3^S.

Phase diagram. Figure 6 represents magnetic phase diagram of Cu_2OSeO_3 constructed using the above analyses. We have shown that spin-flip caused by the development of strain (refer to Fig. 2) may lead to different Hamiltonian below H_2^S and below 50 K. Below H_1^S, spins try to align antiferromagnetically, but, due to presence of other competing interactions (as discussed above), the antiferromagnetically coupled spins may also yield helical spin-textures. So, it is quite possible to have two kinds of helical spin textures[45]: (i) helical1 below 50 K, and (ii) helical2 above 50 K. Due to spiral spin texture, the two helical phases may have identical properties. The similar property may not be observed in the M-T isofields due to almost similar spin texture in helical1 and helical2 phases. Metamagnetic phase transition occurs from H_1^S to H_2^S yielding metamagnetic hysteretic field range. The spins of metamagnetic hysteretic field range may form helical or conical or mixed spin texture[71]. On comparison with previous reports[35,42–45], it is found that the LTS phase emerges in the field range over which meta-

magnetic hysteresis has been observed. Due to discontinuous spin-flip, ring intensity pattern may be observed in SANS. This ring intensity pattern may be the measure of coexistence of other spin-textures, such as spiral and tilted-conical, in LTS phase[42]. In analogy with FD phase[46,47], the metamagnetic hysteretic field range may have field-induced spin-fluctuation. After H_2^S, the weakly bound Cu1 spins get flipped (Fig. 2) completely, and conical phase emerges due to presence of other competing energies. Thus, below H_2^S and 50 K, the physics of Cu_2OSeO_3 will be governed by J_1 (strong FM), J_2 (strong AFM), J_3 (weak AFM), and J_4 (weak FM). Above H_2^S and 50 K, the physics of Cu_2OSeO_3 will be governed by J_1 (strong FM), J_2 (strong AFM), J_3 (weak FM), and J_4 (weak AFM). Below H_2^A, Arrott-plots show negative slopes. So, it can be inferred that the conical phase may have different properties below and above H_2^A. The conical phase continuously transform into field polarized ferrimagnetic phase around H_3^S. It is possible that DMI may become ineffective above H_3^S due to Zeeman energy and spin reorientation. And, DMI may become negligibly small (or zero) above H_3^A leading to saturation magnetization[41] as shown in Fig. 4. HTS phase has been observed in the conical phase in a small window of applied field and temperature[1–8,35,42–45]. The physics of the shaded region (53–61 K) has been explained comprehensively in previous reports[40,41]. A tricritical point (50 K, 9 mT) has been observed where metamagnetic hysteretic field range ceases to exist.

Conclusion

Investigation of the unusual variation of the magnetic moment of the M-T curves confirms the flipping of spins due to the development of strain which causes change in effective anisotropies at low temperature. The crossover from weak FM to weak AFM causes first-order metamagnetic transition leading to the formation of metamagnetic hysteretic field region between helical and conical spin textures. LTS phase with added spiral and tilted-conical phases may have been observed in the metamagnetic hysteretic field range. Arrott-plots analyses confirm that there may exist conical phases having different properties. Also, same (positive or negative) slope regions of Arrott-plots may represent different phases if the slopes vary with different rates. The point (~ 50 K, ~ 9 mT) leads to the tricritical point where first-order metamagnetic hysteretic phase ceases to exist and second-order helical to conical phase transition starts. Finally, a magnetic phase diagram of Cu_2OSeO_3 has been constructed using the above analyses. Further investigations are required to explore the physics of different properties of LTS phase when compared with HTS phase.

Data availability

The data that support the findings of this study are available from the corresponding author upon reasonable request.

Received: 28 May 2022; Accepted: 7 September 2022
Published online: 24 September 2022

References

1. Mühlbauer, S. *et al.* Skyrmion lattice in a chiral magnet. *Science* **323**, 915 (2009).
2. Wilhelm, H. *et al.* Precursor phenomena at the magnetic ordering of the cubic helimagnet FeGe. *Phys. Rev. Lett.* **107**, 127203 (2011).
3. Münzer, W. *et al.* Skyrmion lattice in the doped semiconductor $Fe_{1-x}Co_xSi$. *Phys. Rev. B* **81**, 041203(R) (2010).
4. Seki, S., Yu, X. Z., Ishiwata, S. & Tokura, Y. Observation of skyrmions in a multiferroic material. *Science* **336**, 198 (2012).
5. Fujima, Y., Abe, N., Tokunaga, Y. & Arima, T. Thermodynamically stable skyrmion lattice at low temperatures in a bulk crystal of lacunar spinel GaV_4Se_8. *Phys. Rev. B* **95**, 180410(R) (2017).
6. Kézsmárki, I. *et al.* Néel-type skyrmion lattice with confined orientation in the polar magnetic semiconductor GaV_4S_8. *Nat. Mater.* **14**, 1116–1122 (2015).
7. Kurumaji, T. *et al.* Néel-Type skyrmion lattice in the tetragonal polar magnet $VOSe_2O_5$. *Phys. Rev. Lett.* **119**, 237201 (2017).
8. Adams, T. *et al.* Long-wavelength helimagnetic order and skyrmion lattice phase in Cu_2OSeO_3. *Phys. Rev. Lett.* **108**, 237204 (2012).
9. Fert, A., Reyren, N. & Cros, V. Magnetic skyrmions: Advances in physics and potential applications. *Nat. Rev. Mater.* **2**, 201731 (2017).
10. Jiang, W. *et al.* Skyrmions in magnetic multilayers. *Phys. Rep.* **704**, 1–49 (2017).
11. Yu, X., Tokunaga, Y., Taguchi, Y. & Tokura, Y. Variation of topology in magnetic bubbles in a colossal magnetoresistive manganite. *Adv. Mater.* **29**, 1603958 (2016).
12. Yu, X. *et al.* Magnetic stripes and skyrmions with helicity reversals. *Proc. Natl. Acad. Sci. USA* **109**, 8856 (2012).
13. Yu, X. Z. *et al.* Biskyrmion states and their current-driven motion in a layered manganite. *Nat. Commun.* **5**, 3198 (2014).
14. Qian, F. *et al.* Phase diagram and magnetic relaxation phenomena in Cu_2OSeO_3. *Phys. Rev. B* **94**, 064418 (2016).
15. Pfleiderer, C. Surfaces get hairy. *Nat. Phys.* **7**, 673 (2011).
16. Nagaosa, N. & Tokura, Y. Topological properties and dynamics of magnetic skyrmions. *Nat. Nanotech.* **8**, 899–911 (2013).
17. Fert, A., Cros, V. & Sampaio, J. Skyrmions on the track. *Nat. Nanotech.* **8**, 152 (2013).
18. Tiwari, J. K., Chauhan, H. C., Kumar, B. & Ghosh, S. 3D-Ising like ferromagnetism in skyrmionic bubble host infinite-layer $La_{0.825}Sr_{0.175}MnO_3$ manganite perovskite. *J. Phys.: Condens. Matter* **32**, 195803 (2020).
19. Tiwari, J. K., Kumar, B., Chauhan, H. C. & Ghosh, S. Critical scaling and magnetic phase diagram of bi-skyrmion host quasi-two-dimensional $La_{1.37}Sr_{1.63}Mn_2O_7$ bi-layer manganite. *J. Magn. Magn. Mater.* **535**, 168020 (2021).
20. Dzyaloshinskii, I. A thermodynamic theory of "weak" ferromagnetism of antiferromagnetics. *J. Phys. Chem. Solids* **4**, 241 (1958).
21. Moriya, T. Anisotropic superexchange interaction and weak ferromagnetism. *Phys. Rev.* **120**, 91 (1960).
22. Saratz, N. *et al.* Critical exponents and scaling invariance in the absence of a critical point. *Nat. Commun.* **7**, 13611 (2016).
23. Lin, Y. S., Grundy, P. J. & Giess, E. A. Bubble domains in magnetostatically coupled garnet films. *Appl. Phys. Lett.* **23**, 485 (1973).
24. Fang, Y., Wu, S., Zhu, Z. & Guo, G. Large magneto-optical effects and magnetic anisotropy energy in two-dimensional $Cr_2Ge_2Te_6$. *Phys. Rev. B* **98**, 125416 (2018).
25. Yang, J. H. *et al.* Strong Dzyaloshinskii–Moriya interaction and origin of ferroelectricity in Cu_2OSeO_3. *Phys. Rev. Lett.* **109**, 107203 (2012).
26. Janson, O. *et al.* The quantum nature of skyrmions and half-skyrmions in Cu_2OSeO_3. *Nat. Commun.* **5**, 5376 (2014).
27. Portnichenko, P. Y. *et al.* Magnon spectrum of the helimagnetic insulator Cu_2OSeO_3. *Nat. Commun.* **7**, 10725 (2016).
28. Malozemoff, A. P. Heisenberg-to-Ising crossover in a random-field model with uniaxial anisotropy. *Phys. Rev. B* **37**, 7673 (1988).

29. Malozemoff, A. P. Mechanisms of exchange anisotropy (invited). *J. Appl. Phys.* **63**, 3874 (1988).
30. Daalderop, G. H. O., Kelly, P. J. & Schuurmans, M. F. H. Magnetocrystalline anisotropy and orbital moments in transition-metal compounds. *Phys. Rev. B* **44**, 12054(R) (1991).
31. Hoffer, G. & Strnat, K. Magnetocrystalline anisotropy of YCo_5 and Y_2Co_{17}. *IEEE* **2**, 487–489 (1966).
32. Daalderop, G. H. O., Kelly, P. J. & Schuurmans, M. F. H. First-principles calculation of the magnetocrystalline anisotropy energy of iron, cobalt, and nickel. *Phys. Rev. B* **41**, 11919 (1990).
33. Dubowik, J. Erratum: Shape anisotropy of magnetic heterostructures [Phys. Rev. B 54, 1088 (1996)]. *Phys. Rev. B* **62**, 727 (2000).
34. Lu, Y. *et al.* Shape-anisotropy-controlled magnetoresistive response in magnetic tunnel junctions. *Appl. Phys. Lett.* **70**, 2610 (1997).
35. Qian, F. *et al.* New magnetic phase of the chiral skyrmion material Cu_2OSeO_3. *Sci. Adv.* **4**, eaat7323 (2018).
36. White, J. S. *et al.* Electric field control of the skyrmion lattice in Cu_2OSeO_3. *J. Phys. Condens. Matter* **24**, 432201 (2012).
37. Grigoriev, S. V., Sukhanov, A. S. & Maleyev, S. V. From spiral to ferromagnetic structure in B20 compounds: Role of cubic anisotropy. *Phys. Rev. B* **91**, 224429 (2015).
38. Bauer, A., Garst, M. & Pfleiderer, C. Specific heat of the skyrmion lattice phase and field-induced tricritical point in MnSi. *Phys. Rev. Lett.* **110**, 177207 (2013).
39. Qian, F. *et al.* Phase diagram and magnetic relaxation phenomena in Cu_2OSeO_3. *Phys. Rev. B* **94**, 064418 (2016).
40. Chauhan, H. C., Kumar, B., Tiwari, J. K. & Ghosh, S. Multiple phases with a tricritical point and a Lifshitz point in the skyrmion host Cu_2OSeO_3. *Phys. Rev. B* **100**, 165143 (2019).
41. Chauhan, H. C., Kumar, B., Tiwari, A., Tiwari, J. K. & Ghosh, S. Different critical exponents on two sides of a transition: Observation of crossover from Ising to Heisenberg exchange in skyrmion host Cu_2OSeO_3. *Phys. Rev. Lett* **128**, 015703 (2022).
42. Bannenberg, L. J. *et al.* Multiple low-temperature skyrmionic states in a bulk chiral magnet. *npj Quantum Mater.* **4**, 11 (2019).
43. Halder, M. *et al.* Thermodynamic evidence of a second skyrmion lattice phase and tilted conical phase in Cu_2OSeO_3. *Phys. Rev. B* **98**, 144429 (2018).
44. Chacon, A. *et al.* Observation of two independent skyrmion phases in a chiral magnetic material. *Nat. Phys.* **14**, 936–941 (2018).
45. Aqeel, A. *et al.* Microwave spectroscopy of the low-temperature skyrmion state in Cu_2OSeO_3. *Phys. Rev. Lett.* **126**, 017202 (2021).
46. Kindervater, J. *et al.* Weak crystallization of fluctuating skyrmion textures in MnSi. *Phys. Rev. X* **9**, 041059 (2019).
47. Janoschek, M. *et al.* Fluctuation-induced first-order phase transition in Dzyaloshinskii–Moriya helimagnets. *Phys. Rev. B* **87**, 134407 (2013).
48. Brazovskii, S. A. Phase transition of an isotropic system to a nonuniform state. *Sov. Phys. JETP* **41**, 85 (1975).
49. Bos, J.-W.G., Colin, C. V. & Palstra, T. T. M. Magnetoelectric coupling in the cubic ferrimagnet Cu_2OSeO_3. *Phys. Rev. B* **78**, 094416 (2008).
50. Seki, S. *et al.* Formation and rotation of skyrmion crystal in the chiral-lattice insulator Cu_2OSeO_3. *Phys. Rev. B* **85**, 220406(R) (2012).
51. Liu, G. J. & Sun, J. R. Determination of the entropy changes in the compounds with a first-order magnetic transition. *Appl. Phys. Lett.* **90**, 032507 (2007).
52. Deppe, M. *et al.* Pronounced first-order metamagnetic transition in the paramagnetic heavy-fermion system CeTiGe. *Phys. Rev. B* **85**, 060401(R) (2012).
53. Zhang, Y. Q., Zhang, Z. D. & Aarts, J. Erratum: First-order nature of a metamagnetic transition and mechanism of giant magnetoresistance in $Mn_2Sb_{0.95}Sn_{0.05}$ [Phys. Rev. B 70, 132407 (2004)]. *Phys. Rev. B* **71**, 229902 (2005).
54. Stryjewski, E. & Giordano, N. Metamagnetism. *Adv. Phys.* **26**(5), 487–650 (2006).
55. Zhang, F. *et al.* Super-exchange theory for polyvalent anion magnets. *New J. Phys.* **21**, 053033 (2019).
56. Mondal, D. *et al.* Crossover from antiferromagnetic to ferromagnetic exchange coupling in a new family of bis-(μ-phenoxido) dicopper(II) complexes: A comprehensive magneto-structural correlation by experimental and theoretical study. *ACS Omega* **4**, 10558 (2019).
57. Conduit, G. J., Green, A. G. & Simons, B. D. Inhomogeneous phase formation on the border of itinerant ferromagnetism. *Phys. Rev. Lett.* **103**, 207201 (2009).
58. Joy, P. A., Kumar, P. S. A. & Date, S. K. The relationship between field-cooled and zero-field-cooled susceptibilities of some ordered magnetic systems. *J. Phys.: Condens. Matter* **10**, 11049 (1998).
59. Wang, X. H., Peng, W. K. & Lew, W. S. Flux-closure chirality control and domain wall trapping in asymmetric magnetic ring. *J. Appl. Phys.* **106**, 043905 (2009).
60. Shepley, P. M., Rushforth, A. W., Wang, M., Burnell, G. & Moore, T. A. Modification of perpendicular magnetic anisotropy and domain wall velocity in Pt/Co/Pt by voltage-induced strain. *Sci. Rep.* **5**, 7921 (2015).
61. Seo, Soo-Man., Lee, Kyung-Jin., Jung, Soon-Wook. & Lee, Hyun-Woo. Controllable chirality switching of a moving domain wall by oblique magnetic field. *Appl. Phys. Lett.* **97**, 032507 (2010).
62. Zhang, L. *et al.* Critical behavior of the single-crystal helimagnet MnSi. *Phys. Rev. B* **91**, 024403 (2015).
63. Jiang, W., Zhou, X. Z. & Williams, G. Scaling the anomalous Hall effect: A connection between transport and magnetism. *Phys. Rev. B* **82**, 144424 (2010).
64. Zhang, L. *et al.* Critical phenomenon of the near room temperature skyrmion material FeGe. *Sci. Rep.* **6**, 22397 (2016).
65. Mϕrup, S. & Frandsen, C. Thermoinduced magnetization in nanoparticles of antiferromagnetic materials. *Phys. Rev. Lett.* **92**, 217201 (2004).
66. Van Vleck, J. H. On the theory of antiferromagnetism. *J. Chem. Phys.* **9**, 85 (1941).
67. Evans, D. M., Schiemer, J. A., Schmidt, M., Wilhelm, H. & Carpenter, M. A. Defect dynamics and strain coupling to magnetization in the cubic helimagnet Cu_2OSeO_3. *Phys. Rev. B* **95**, 094426 (2017).
68. Belesi, M. *et al.* Magnetoelectric effects in single crystals of the cubic ferrimagnetic helimagnet Cu_2OSeO_3. *Phys. Rev. B* **85**, 224413 (2012).
69. Perry, R. S. *et al.* Multiple first-order metamagnetic transitions and quantum oscillations in ultrapure $Sr_3Ru_2O_7$. *Phys. Rev. Lett.* **92**, 166602 (2004).
70. Lyubina, J., Nenkov, K., Schultz, L. & Gutfleisch, O. Multiple metamagnetic transitions in the magnetic refrigerant $La(Fe, Si)_{13}H_x$. *Phys. Rev. Lett.* **101**, 177203 (2008).
71. Gama, S. *et al.* A general approach to first order phase transitions and the anomalous behavior of coexisting phases in the magnetic case. *Adv. Funct. Mater.* **19**, 942 (2009).
72. Arrott, A. Criterion for ferromagnetism from observations of magnetic isotherms. *Phys. Rev.* **108**, 1394 (1957).
73. Banerjee, B. K. On a generalised approach to first and second order magnetic transitions. *Phys. Lett.* **12**, 16 (1964).

Acknowledgements

We thank AIRF-JNU for providing facilities for PPMS and XRD measurements. H.C.C. acknowledges UGC-CSIR for financial support through fellowship. This project is partially supported by SERB, Department of Science and Technology, Government of India, through the project with SERB sanction order no. CRG/2021/000776.

Author contributions

S.G. conceived the problem. H.C.C. and B.K. performed the experiments. H.C.C. wrote the main manuscript text. All authors reviewed the manuscript.

Competing interests

The authors declare no competing interests.

Additional information

Correspondence and requests for materials should be addressed to S.G.

Reprints and permissions information is available at www.nature.com/reprints.

Publisher's note Springer Nature remains neutral with regard to jurisdictional claims in published maps and institutional affiliations.